

Hierarchical Coordinated Fast Frequency Control using Inverter-Based Resources

Etinosa Ekomwenrenren, *Student Member, IEEE*, Zhiyuan Tang, *Member, IEEE*,
John W. Simpson-Porco, *Member, IEEE*, Evangelos Farantatos, *Senior Member, IEEE*,
Mahendra Patel, *Fellow, IEEE*, and Hossein Hooshyar, *Senior Member, IEEE*

Abstract—The share of inverter-connected renewable energy resources (RESs) is increasing in the grid, with these resources partially displacing conventional synchronous generators. This has resulted in increased variability of active power supply, reduced overall inertia, and increased spatial heterogeneity of inertia, leading to faster system frequency dynamics along with larger and more frequent frequency control events. These effects are expected to become increasingly more important in power system control in next-generation grids, which may conceivably be made up entirely of RESs. To mitigate these challenges, a fast, area-based hierarchical control strategy is proposed. This scheme partitions the power system into small areas, estimates local power imbalances, and corrects them by utilizing local inverter-based resources (IBRs). In cases where sufficient resources are not available locally, power is preferentially sourced from electrically close neighbours using an iterative distributed optimization scheme which preserves information privacy between areas. The proposed frequency control architecture can be retrofit onto existing control systems, and allows for flexibility in the amount of model information available to the designer. The control strategy is validated on two detailed multi-area power system models. Simulation results show that the strategy provides fast and localized frequency control.

Index Terms—frequency control, low inertia, distributed control, renewable energy, smart grid, next generation control.

I. INTRODUCTION

SPURRED by climate change concerns, the world is moving towards a low-carbon future, and countries have set ambitious climate change targets in order to limit the global temperature rise [1]. Decarbonizing the power sector is essential in meeting these climate change goals and requires raising the share of renewables in the world’s primary energy supply from the current 15% to 65% [1]. The increasing penetration of these intermittent and variable renewable energy sources (RES, mostly inverter-connected wind and solar plants) is resulting in increased net load variability. Additionally, RES are displacing traditional synchronous generators from the power grid, along with the stored kinetic energy they provide through inertia. The ensuing reduction in the system rotational inertia

can significantly impact power system operation and stability, resulting in large frequency deviations, faster frequency dynamics, and heterogeneous inertia distribution throughout the system [2], [3], [4], [5]. Low-inertia stability issues are now manifesting in the real world; for example, the increasing penetration of inverter-connected RES has been blamed for the recent power system blackout in South Australia [6].

The setting envisaged in this work is in next-generation grids, where the increased penetration of IBRs will play an outsized role in power system control, and where generation may even be composed entirely of RESs. In these grids, sensing ability and control authority will be dispersed over many more devices than in the past, making decentralization increasingly important in managing the resulting information flows. Together with the intermittency, load variability and uncertainty introduced by distributed energy resources [2], [5], it would become increasingly essential for control paradigms that incorporate very fast localized control with high-bandwidth wide-area coordination. These high-bandwidth control schemes will become increasingly feasible as the grid modernizes, with communication infrastructure playing a dominant role [7], [8]. Advances in remote communication and sensing with the use of global positioning system (GPS) synchronized phasor measurements units (PMUs) will allow for improved monitoring and protection [7], enabling fast control actions using IBRs [8].

This paper presents a real-time frequency control scheme to exploit these improvements in modern grid monitoring and communication infrastructure by using IBRs. Although the current mechanisms being considered for facilitating increased penetration of inverter-connected RES tacitly assume that conventional generation continues to supply needed grid support services such as frequency control, those essential grid support services will increasingly need to come from these inverter-interfaced RES as systems evolve to rely more heavily on them. In this case, there will be increasing need to demphasize operating these IBRs at their maximum power limits in lieu of providing these grid support services [9], [10] and we envisage that dedicated IBRs will be available to provide regulation services in the ancillary services market [11], [9], [10]. Frequency control methods along similar lines have been recently proposed in the literature. We will discuss such methods and provide a brief literature overview of issues pertaining to the prevalence of inverter-connected RES in the grid. More detailed discussions on the strategies can be found in [12].

E. Ekomwenrenren and Z. Tang are with the Department of Electrical and Computer Engineering, University of Waterloo, Waterloo, ON N3L 3G1 CA (e-mail: etinosa.ekomwenrenren@uwaterloo.ca; zhiyuan.tang@uwaterloo.ca).

J. W. Simpson-Porco is with the Department of Electrical and Computer Engineering, University of Toronto, 10 King’s College Road, Toronto, ON, M5S 3G4, CA (e-mail: jwsimpson@ece.utoronto.ca)

E. Farantatos, M. Patel, and H. Hooshyar are with the Electric Power Research Institute, Palo Alto, CA 94304 USA (e-mail: efarantatos@epri.com; mpatel@epri.com; hhooshyar@epri.com).

Funded under EPRI Project #10009168: Wide-Area Hierarchical Frequency and Voltage Control for Next Generation Transmission Grids.

Several authors have investigated the impact of the increasing penetration of inverter-connected RES on power system and proposed various control schemes. Authors in [2], [4], [3] investigated the impact of low-inertia on power systems stability, operation, and frequency control in detail and the emerging issue of inertia heterogeneity on frequency dynamics was explored in [13]. Still other works have focused on fast frequency response (FFR) methods for low-inertia systems, which focuses on providing controlled frequency support to the system by acting rapidly on a frequency measure to compensate for the lost inertial and governor-turbine response from conventional synchronous generators. Authors in [14], [15] investigated fast frequency support using multi-terminal direct current (MTDC) schemes, which utilize the energy transferred from wind turbine rotating mass and stored within direct current (DC) links. Authors in [16], [17] and [18], [19] propose methods for fast injection and control of active power from photovoltaic systems and doubly-fed induction generator based wind turbines, respectively, to support system frequency. In [20], [21], authors present methods in utilizing energy storage for fast frequency support. While these works demonstrate the need for FFR in low-inertia grids and investigate the potential of utilizing a range of emerging technologies in providing it, they are mostly focused on the specific technology or energy source being considered. As the grid and its associated technologies are still evolving, there is a need for a technology-agnostic, modular framework that would provide fast frequency control while optimally coordinating the available grid resources.

Modern approaches to power system frequency control can be roughly divided into three categories: model predictive control (MPC), adaptive control, and miscellaneous methods for coordinated dispatch. Control schemes based on MPC have been proposed in several studies [22], [23], [24], [25]. Although MPC-based approaches have the desirable feature of constraint satisfaction during transients, this benefit relies heavily on accuracy of the system model, and the resulting control laws place a heavy communication burden for real-time implementation.

Traditional frequency control based on automatic generation control (AGC) [26], [27] usually requires extensive tuning of the AGC's proportional integral (PI) controllers to obtain good performance and stable operation. Authors in [28] propose an adaptive controller that seeks to automate this tuning process by computing and applying a correction in real-time. Other adaptive approaches [29], [12], aim to tackle the frequency control problem by minimizing the need for a system model by using techniques based on dynamic programming and artificial intelligence. However, it is usually difficult to assess the stability of these controllers. There has also been high profile failures of implemented adaptive controllers [30].

The final category seeks to provide frequency support to the system by utilizing fast acting inverter-based resources. Authors in [31] have proposed a load frequency controller which provides frequency control by adjusting the setpoints of distributed energy resources by means of direct observation of active power generation and consumption. Despite this method's advantages over the traditional AGC, it requires

a high degree of monitoring infrastructure and total grid visibility.

Another approach in the same category is the wide-area monitoring and control scheme proposed by researchers in [5], [32]. In the scheme, a central authority, operating on a slow time-scale, coordinates and optimizes geographically dispersed local controllers, which receive measurements from PMUs and dispatch controllable active power resources to mitigate the effect of disturbances. However, the work does not investigate the stability or robustness of the scheme. Furthermore, although measurements are collected regionally, control is still based on a system-wide frequency estimate, which may not effectively address the issue of inertia heterogeneity. Finally, the central authority, as it receives the status and resource limits of all resources, has system-wide visibility which raises privacy issues and may limit the distributed implementation.

A. Contributions

Our proposed scheme aims to address the shortcomings of the aforementioned strategies. We leverage well-understood control-theoretic principles for advanced design (Section II), relying only on simple system models (Section II). Our scheme uses easily accessible local area information (Section II-A), and the designer may safeguard data-ownership and privacy between areas (Section III-B).

We develop, analyze, and numerically test a two-layer local-global IBR control scheme to provide fast and localized response to frequency events, such as load changes (IV-A, IV-B) and generation trips (IV-D). In our scheme, a power system is partitioned into geographically small (e.g., several substations) local control areas (LCAs), within which high-bandwidth low-latency measurements are available for local decision making. For each LCA we design a fast local disturbance estimation and rejection control loop (Section II), loosely based on the principle of internal model control. The local control loop processes local measurements and quickly re-dispatches local IBRs to balance local generation and net load. We provide theoretical analysis results to support the design procedure.

From the produced disturbance estimate, the local re-dispatching of the IBRs is formulated as a simple optimization problem (Section III-A). For contingent situations where LCA IBR resources are insufficient, we design a higher-level central coordinating controller, to facilitate the transfer of additional power from electrically close neighbouring areas on a slower time-scale (Section III-B). In Section IV, our results are extensively validated via simulations on two detailed power system models; several scenarios are examined, including load increases, generation trips, and three-phase faults.

The novelty of our methodology lies in the rapid and accurate re-dispatch of fast IBRs to compensate unmeasured net-load changes, and in the layered control architecture, which enables fast, localized control in response to local power imbalances with supplementary wide-area coordination. This hierarchical architecture provides flexibility in designing the constituent layers, while local handling of information allows for faster speed and efficiency of control response. Our scheme has the following appealing characteristics:

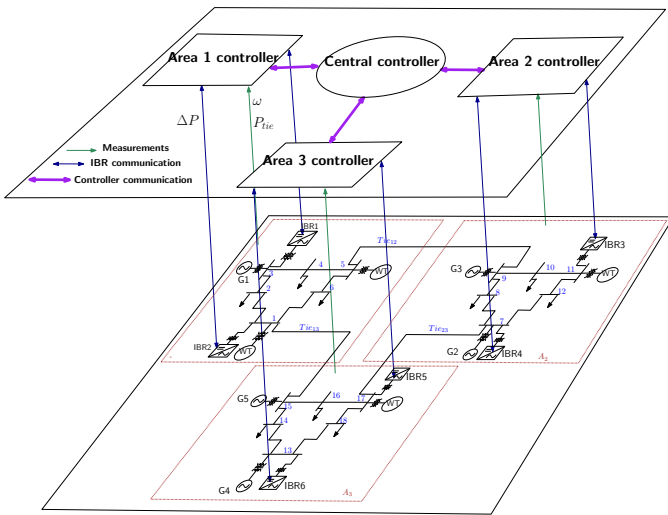


Fig. 1: Cyber-physical system illustrating frequency control approach.

- 1) *Practicality*: the design for each LCA is based only on a simple aggregated area model, although the designer is free to incorporate a more detailed model if one is available. This is advantageous, since owing to the increasing power system scale, complexity and changing dynamics, ensuring the accuracy of complex system models is a major challenge in practice. All controller computations are either linear update rules or small, simple optimization problems. Furthermore, due to the robustness against model uncertainty provided by the feedback configuration, the scheme affords the designer a large margin of error in the accuracy of this model, which is indispensable in practice as even lumped parameters can be difficult to estimate; see Section IV-E. Finally, the design can be retrofit onto existing systems.
- 2) *Localized and fast control*: The local control loops take into account local communication delays, inertia, and primary frequency response characteristics, and use only local measurements of frequency and line power flows. An upshot of this localized use of measurements is the minimization of latency. This use of local measurements together with the more granular partitioning of the system, allows for the quick localization of net power imbalance and redispatch of fast-acting IBRs for its correction, resulting in fast frequency regulation.
- 3) *Multi-area data privacy*: Potentially sensitive information such as device limits, set-points, and available spare capacity of resources in an LCA are not shared with either the central controller or the neighboring LCAs. Furthermore, computation of control actions for the additional power adjustments are done *within* each LCA (14), with the central controller providing minimal coordination between LCAs.

II. AN INTERNAL MODEL CONTROL APPROACH FOR LOCAL AREA-BASED FREQUENCY CONTROL

We assume that the power system is partitioned into small local control areas (LCAs), with the goal being for local resources in each area to correct local net load imbalances. This shrinking of the spatial scale permits increasing decentralization of control actions, and is enabled by the expected deployment of more sensing and inverter-based resources within the system. The overall hierarchical IBR control architecture using a three-area power system is sketched in Figure 1. The power system consists of 18 buses, 36 transmission lines, and 15 generators. The generators consist of 5 conventional synchronous generators, 4 wind generation plants (WT), and 6 generating units representing generic inverter-based resources whose inertias are fully decoupled from the grid. Our design involves a local controller for each area, which acts on power and frequency measurements and re-dispatches IBRs to correct local net-load load imbalances. Finally, a central controller coordinates the activities of all LCA controllers in the system to ensure satisfaction of the global objectives.

In this section, we focus on just one such area. Our goal is to design an area-wise decentralized controller which uses only local measurements to correct any power imbalance within the LCA by quickly re-dispatching local IBRs. Our design is based on the idea of disturbance estimation and rejection, and can be interpreted as an implementation of the classical internal model control (IMC) paradigm [33] for internally stable systems.

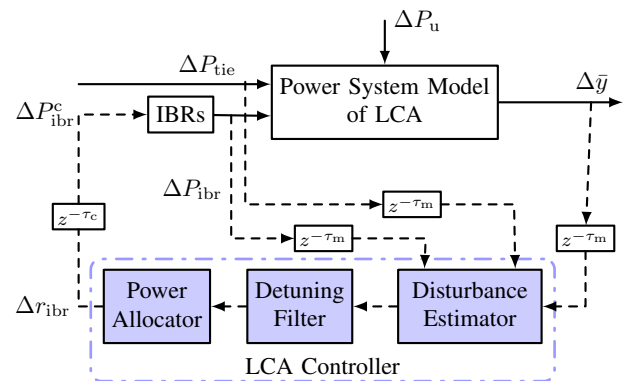


Fig. 2: Block diagram of area control structure for each LCA. Dashed lines denote sampled signals.

Our local controller design is based on the block diagram shown in Figure 2. The local frequency controller consists of the disturbance estimator, optional detuning filters, and a power allocator. The disturbance estimator processes system measurements to produce an estimate $\Delta\hat{P}_u$ of the unmeasured net active power change in the LCA, relative to the current dispatch point. This imbalance is then allocated to IBRs within the area. We detail the design of disturbance estimator and detuning filter here, while covering optimal power allocation in the next section.

A. Local Disturbance Estimator for the LCA

The starting point for disturbance estimation is a nominal (small-signal) dynamic model of the LCA dynamics at the current dispatch point. As each LCA represents a very small part of the overall interconnection, it is reasonable that a dynamic model can be locally built and maintained; the accuracy of this nominal model may vary based on the level of detailed system component models available, and one may even wish to fit this model from historical or experimental data. For practical reasons, it is desirable to use the simplest model which captures the primary frequency response dynamics for design purposes, and as such, we restrict our attention to *lumped LCA models*, where all power injections are assumed to occur at a single electrical point. We generically express the lumped small-signal model of the LCA as

$$\Delta \dot{x} = \tilde{A}\Delta x + \tilde{B}_1 \Delta P_{\text{ibr,tot}}^c + \tilde{B}_2 (\Delta P_{\text{tie}} + \Delta P_{\text{u}}) \quad (1)$$

where \tilde{A} is a Hurwitz stable matrix. In (1), Δx is the internal state vector of the area, which could model, for example, generator, load, and IBR dynamics. The control input $\Delta P_{\text{ibr,tot}}^c$ is the sum of all command changes to IBRs. The measurable disturbance ΔP_{tie} is the sum of all deviations in LCA tie flows, and ΔP_{u} is the net unmeasurable active power imbalance in the LCA. The model (1) is a general state-space representation of any LCA model that can be used for *design purposes*, as illustrated in Figure 2, and is distinct from the detailed models of the test power systems used in validating the proposed scheme, which are discussed in Section IV. We discretize (1) using the zero-order-hold method with a chosen sampling period T_s , yielding a discrete-time model

$$\Delta x^{k+1} = A\Delta x^k + B_1 \Delta P_{\text{ibr,tot}}^{c,k} + B_2 (\Delta P_{\text{tie}}^k + \Delta P_{\text{u}}^k), \quad (2)$$

where A is Schur stable and k is the sampling instant index. The IBR commands $\Delta P_{\text{ibr,tot}}^{c,k}$ are subject to communication delays, which for modelling purposes we assume are fixed at τ_c sample periods. This can be integrated directly into the model by appending extra states $\Delta \eta_c$ governed by

$$\Delta \eta_c^{k+1} = A_c \Delta \eta_c^k + B_c \Delta r_{\text{ibr,tot}}^k, \quad \Delta P_{\text{ibr,tot}}^{c,k} = C_c \Delta \eta_c^k, \quad (3)$$

where (A_c, B_c, C_c) is a state-space realization of a τ_c -step delay. The unknown net active power imbalance is modelled via a difference equation with unknown initial condition [34], [35]. The simplest choice is the constant disturbance model

$$\Delta P_{\text{u}}^{k+1} = \Delta P_{\text{u}}^k. \quad (4)$$

More complex versions of (4) require only minor extensions. Moreover, if some load changes are measurable in real-time, this can also be incorporated by adding appropriate feedforward signals to the IBR commands; the details are omitted. The vector of system measurements that we can use for estimation are

$$\Delta \bar{y}^k = C \Delta x^k. \quad (5)$$

These measurements should include frequency deviation, but may include other variables such as power outputs and voltages, if available. Measurement delays are again incorporated by appending extra states $\Delta \eta_m$ as

$$\Delta \eta_m^{k+1} = A_m \Delta \eta_m^k + B_m \Delta \bar{y}^k, \quad \Delta y^k = C_m \Delta \eta_m^k \quad (6)$$

where (A_m, B_m, C_m) is a state-space realization of a τ_m -step delay for each measurement. Combining (2)–(6), the overall model of the LCA with states $\Delta \xi = (\Delta x, \Delta P_{\text{u}}, \Delta \eta_c, \Delta \eta_m)$, inputs $\Delta v = (\Delta r_{\text{ibr,tot}}, \Delta P_{\text{tie}})$, and delayed measurements Δy is given by

$$\Delta \xi^{k+1} = \mathcal{A} \Delta \xi^k + \mathcal{B} \Delta v^k, \quad \Delta y^k = \mathcal{C} \Delta \xi^k \quad (7)$$

where $\mathcal{C} = [0 \ 0 \ 0 \ C_m]$ and

$$\mathcal{A} = \begin{bmatrix} A & B_2 & B_1 C_c & 0 \\ 0 & 1 & 0 & 0 \\ 0 & 0 & A_c & 0 \\ B_m C & 0 & B_m C_c & A_m \end{bmatrix}, \quad \mathcal{B} = \begin{bmatrix} 0 & B_2 \\ 0 & 0 \\ B_c & 0 \\ 0 & B_m \end{bmatrix}.$$

The following result (proof in Appendix A) establishes that this extended model is detectable.

Proposition II.1 (Detectability of Area Model (7)). *Assume that A is Schur stable and that $\begin{bmatrix} A^{-I} & B_2 \\ C & 0 \end{bmatrix}$ has full column rank. Then $(\mathcal{C}, \mathcal{A})$ is detectable.*

The rank condition in Proposition II.1 stipulates that the transfer matrix from ΔP_{u} to $\Delta \bar{y}$ has no transmission zeros at $z = 1$; this will hold as long as a frequency deviation from within the LCA is one of the measured variables. It follows from linear systems theory that we can design a dynamic state estimator [36] for (7):

$$\begin{aligned} \Delta \hat{\xi}^{k+1} &= \mathcal{A} \Delta \hat{\xi}^k + \mathcal{B} \Delta v^k + \mathcal{L} (\mathcal{C} \Delta \hat{\xi}^k - \Delta y^k) \\ \Delta \hat{P}_{\text{u}}^k &= [0 \ 1 \ 0 \ 0] \Delta \hat{\xi}^k, \end{aligned} \quad (8)$$

where \mathcal{L} is the estimator gain matrix which can be designed by, e.g., linear-quadratic optimal methods. The estimator produces the desired running estimate $\Delta \hat{P}_{\text{u}}^k$ of the unknown net active power imbalance, which can now be allocated to the IBRs.

Remark II.2 (Detuning for Robust Stability). *In the presence of significant model uncertainty, one may wish to “slow down” the overall control loop to ensure robust closed-loop stability at the cost of decreased controller bandwidth. This can be achieved by passing the estimated unmeasured net active power change $\Delta \hat{P}_{\text{u}}^k$ through a discrete low-pass filter*

$$F_{\text{detune}}[z] = \frac{1 - e^{-T_s/\tau_f}}{z - e^{-T_s/\tau_f}} \quad (9)$$

with filter time constant $\tau_f > 0$, and then allocating the result to IBRs. This utility will be illustrated in Section IV. \square

B. System Frequency Response LCA Modelling

For design purposes, a simple and effective model for the LCA dynamics is the following two-state *system frequency response* (SFR) model proposed in [37], [38], which describes the machine mechanical and turbine-governor response. The frequency model represents the averaged system frequency response when all generating units and frequency-responsive loads are viewed as a single aggregate unit. The model, which can be easily put into the general form (1), is¹

¹We have assumed that most of the generating units are reheat steam turbine units and that the dominant time constants are the reheater time constant and the inertia constant; these assumptions can be easily modified.

$$\begin{aligned} 2H\Delta\dot{\omega} &= -(D + \frac{1}{R_I})\Delta\omega + \Delta P_m - \Delta P_u - \Delta P_{tie} + \Delta P_{ibr,tot}^c \\ T_R\Delta\dot{P}_m &= -\Delta P_m - R_g^{-1}(\Delta\omega + T_R F_H \Delta\dot{\omega}), \end{aligned} \quad (10)$$

where $\Delta\omega$ [p.u.] is the area frequency deviation, ΔP_m [p.u.] is the mechanical power change, H [s] is the inertia constant, T_R [s] is the reheat time constant, D [p.u.] is the load damping, F_H the fraction of total power generated by the high pressure turbine, R_g , R_I [p.u.] are the generator and IBRs primary droop constants respectively, where we have simplified the IBRs drop control scheme by eliminating the time constants, since they are significantly faster than the ones of the conventional generators [39].

C. Nominal Stability and Perfect Disturbance Rejection

From Section II-A, the controller for each LCA embeds a dynamic model of the LCA in order to produce a running estimate $\Delta\hat{P}_u^k$ for the local unmeasured disturbance. It follows by more-or-less standard observer-based control theory that if the total IBR power $\Delta P_{ibr,tot}^{c,k}$ in (2) is set equal to the disturbance estimate $\Delta\hat{P}_u^k$ produced by (8), then the closed-loop system (2)–(8) will be internally stable and any constant disturbance will be eliminated, i.e., $\Delta\hat{P}_u^k \rightarrow \Delta P_u$ as $k \rightarrow \infty$. In other words, the design always achieves *nominal* stability and asymptotically eliminates any load net-load imbalance.

Perhaps surprisingly, the net-load mismatch will still be eliminated even when the LCAs are interconnected as in Figure 1 — and will occur irrespective of the model mismatch between the true system and the model used in designing the estimator — as long as the interconnected closed-loop system is stable. To demonstrate this, suppose that the linear time-invariant (LTI) model

$$\begin{aligned} \Delta x_p^{k+1} &= A_p \Delta x_p^k + \sum_j B_{p,j} (\Delta P_{ibr,tot,j}^k - \Delta P_{u,j}^k) \\ \Delta q_i &= (\Delta P_{tie,i}, \Delta \bar{y}_i) \end{aligned}$$

describes the *true* linearized and discretized multi-area power system with measurements q_i for LCA i , where A_p is Schur stable. The aggregated IBR inputs $\Delta P_{ibr,tot,i}^k$ to this model are set equal to the estimates produced by the LCA disturbance estimators (8), which are themselves designed using any approximate model (e.g., the SFR model (10)) of the LCA. We can then show the following; the proof is in Appendix A.

Theorem II.3 (Perfect Disturbance Rejection). *Consider the closed-loop system described above, and assume that the system is internally stable. Then for any constant unmeasured net-load disturbances $\{\Delta P_{u,j}\}$, it holds for each LCA i that $\Delta P_{ibr,tot,i}^k = \Delta\hat{P}_{u,i}^k \rightarrow \Delta P_{u,i}$ as $k \rightarrow \infty$.*

Given Theorem II.3, the key issue becomes whether closed-loop *dynamic* stability and performance is maintained in the presence of model uncertainty, i.e., robust stability and performance. We make two comments. First, robust closed-loop stability can always be achieved by lowering the controller bandwidth as described in Remark II.2; see, e.g., [33]. This will guarantee stability at the possible cost of decreased control performance. Second, while we omit the details, we have

used modern robust control tools [40] to examine stability robustness of the design without controller detuning, when the estimator is designed based on an SFR-type model (10). We have observed guaranteed stability and acceptable performance under up to 10% joint variation in H , T_R , and R_g . Robust control analysis typically results in conservative guarantees, meaning that much more variation can be tolerated in practice before lowering the control bandwidth becomes necessary. We verify these conclusions on a detailed test system in Section IV-E.

Remark II.4 (Key differences with AGC). *There are several key differences between our proposed approach and the traditional power system frequency control (primary control plus the AGC).*

a) *Spatial scale:* In contrast to the large traditional balancing authority areas considered in AGC, which typically contain hundreds of buses and generation sites, the LCAs we consider can be considerably smaller. Many LCAs would be contained within a single balancing authority area, each LCA containing, for instance, several substations. This smaller spatial scale permits further localization of control actions.

b) *Model information:* While maintaining an accurate dynamic model would be prohibitively difficult to do for an entire balancing authority area, the small scale of LCAs permits estimation and continued maintenance of at least a crude dynamic LCA model, accounting for aggregate inertial and primary control/turbine-governor effects. Incorporation of this model (2) into the LCA controller design enables substantially faster estimation of net imbalances compared to the classical frequency bias constant methods used in AGC.

c) *Temporal scale:* The improved local model information described above enables faster and more accurate estimation of local net active power imbalances than is possible in AGC. By combining this fast estimation with fast-acting IBRs as the primary source of compensating power, our scheme is capable of providing fast frequency control within seconds, as opposed to the traditional AGC time scale of minutes.

d) *Inter-LCA coordination:* The AGC is balancing-authority-wise decentralized; no communication occurs during online operation between balancing authorities. As the LCAs considered in our scheme are much smaller than balancing authority areas, it becomes more more important to coordinate and share resources between areas when required. The second layer in our proposed control hierarchy achieves this in a fashion which preserves information privacy between areas. We note that this higher coordination layer of our controller is not itself conceptually analogous to AGC, as the objective is explicitly to procure power from adjacent LCAs in an efficient and privacy-preserving manner.

As a final point, we wish to emphasize that the proposed scheme is fully backwards-compatible with AGC; both can be implemented on the same system — even if IBRs are integrated into AGC — as they operate on very different spatial and temporal scales.

□

III. MATHEMATICAL FORMULATION FOR OPTIMAL POWER ALLOCATION

We now design a power allocation mechanism for the IBRs, completing the frequency controller design from Section II. The net power imbalance estimate $\Delta \hat{P}_u^k$ from the disturbance estimator is used to compute the active power reference for the IBRs in an LCA, subject to the device limits. In Section III-A we formulate this re-dispatch via a simple optimization problem, which is solved locally at each time step by the LCA controller; we call this stage one of the redispatch. If a very large disturbance occurs however, local resources may not be sufficient to maintain power balance. For this situation, in Section III-B we design a privacy-preserving higher-level coordination control layer to optimally coordinate IBR responses from nearby LCAs; we call this stage two of the redispatch.

A. Stage 1: Local Redispatch of IBRs

In stage one, at each sampling instant, the local resources are re-dispatched to compensate for the current net disturbance estimate in each LCA. Let $\mathcal{A} = \{1, \dots, N\}$ index the LCAs, and let $\mathcal{I}_i = \{1, \dots, m_i\}$ index the resources in LCA i . Let $\mathcal{P}_{ij} = [\underline{P}_{ij}, \bar{P}_{ij}]$ denote the power set-point limits for resource j in area i . The new optimal power set-points $\{P_{ij}^*\}_{j \in \mathcal{I}_i}$ for the resources in area i are computed at time step k via

$$\begin{aligned} & \underset{P_{ij} \in \mathcal{P}_{ij}}{\operatorname{argmin}} f(P_{i1}, \dots, P_{im_i}, \varphi_i) \\ & \text{subject to } \sum_{j \in \mathcal{I}_i} (P_{ij} - P_{ij}^{\text{ref}}) + \varphi_i = \Delta \hat{P}_{u,i}^k \end{aligned} \quad (11)$$

where P_{ij}^{ref} denotes the nominal dispatch set-point for the j^{th} resource in area i . The equality constraint models local power balance. The slack variable φ_i ensures feasibility, and its optimal value φ_i^* represents the remaining power mismatch within the LCA after local redispatch, which will be used in Section III. The objective function f captures the cost associated with utilizing the resources in the LCA for disturbance rejection; this may be a monetary cost, or may be designed for operational convenience. As our focus is not on economic or market aspects, for this work, we have selected the following cost function

$$f(P_{i1}, \dots, P_{im_i}, \varphi_i) = \sum_{j \in \mathcal{I}_i} \frac{1}{2} \left(\frac{P_{ij} - P_{ij}^{\text{ref}}}{\bar{P}_{ij} - P_{ij}^{\text{ref}}} \right)^2 + \lambda |\varphi_i|.$$

Minimization of f allocates power to the resources in proportion to their available headroom. When set large enough, the penalty parameter $\lambda > 0$ ensures that φ_i^* is zero when local resources are sufficient to balance the local disturbance. Note that the limits of the devices and the current dispatch set-points are assumed to be available to the LCA controllers. Hence, resources at their maximum operating range and with no available headroom will not be dispatched. The optimization problem (11) can be solved very quickly and reliably at each sampling instant.

B. Stage 2: Coordination Layer for Inter-Area IBR Response

If local resources in LCA $i \in \mathcal{A}$ are insufficient, then from Section III-A, the local mismatch variable φ_i^* will be non-zero. The variables φ_i^* are communicated to a centralized controller (Figure 1), which is tasked with computing an aggregated dispatch adjustment $a_i^* \in \mathbb{R}$ for each LCA via the quadratic program (QP)

$$\min_{\{a_i\}_{i \in \mathcal{A}}} \sum_{i \in \mathcal{A}} q_i a_i^2 \quad (12a)$$

$$\text{s.t. } 0 = \sum_{i \in \mathcal{A}} (a_i - \varphi_i^*) \quad (12b)$$

$$0 \leq a_i \cdot \operatorname{sign} \left(\sum_{i \in \mathcal{A}} \varphi_i^* \right), \quad i \in \mathcal{A} \quad (12c)$$

$$a_i + \sum_{j \in \mathcal{I}_i} P_{ij}^* \in \mathcal{P}_i, \quad i \in \mathcal{A} \setminus \{1\}. \quad (12d)$$

The weight q_i in the objective is designed as

$$q_i := \sum_{j \in \mathcal{A}} |Z_{ij}| w_j, \quad w_j := \frac{|\Delta \hat{P}_{u,j}|}{\epsilon + \sum_{k \in \mathcal{A}} |\Delta \hat{P}_{u,k}|}, \quad (13)$$

where Z_{ij} is the *effective impedance* [41] between LCAs i and j , with $Z_{ii} \equiv 0$ and where $\epsilon > 0$ is small to prevent division by zero. The intuition is that q_i is a weighted average of the distance from LCA i to LCAs where disturbances are significant; a small distance encourages power procurement from LCA i . In essence, areas that are electrically close to the load disturbance will be sourced for additional power. The effective impedance is computed based on a per-phase, per-unit equivalent of the connections between LCAs; see, e.g., [41]. The constraint (12b) ensures global power balance, while (12c) ensures all adjustments are made in the same direction. Finally, (12d) enforces aggregate power limits for each LCA, with the aggregate area constraint set \mathcal{P}_i defined as

$$\mathcal{P}_i = \left[\sum_{j \in \mathcal{I}_i} \underline{P}_{ij}, \sum_{j \in \mathcal{I}_i} \bar{P}_{ij} \right].$$

To ensure feasibility of (12), the first LCA is treated as a slack area. Once (12) is solved, the aggregate IBR dispatch adjustments a_i^* for each LCA are disaggregated by each LCA by locally re-solving (11) with $\Delta \hat{P}_{u,i}$ replaced by $\Delta \hat{P}_{u,i} + a_i^*$.

C. Privacy-Preserving Distributed Implementation of Stage 2

If all data in (12) is available to the central controller, then (12) can be directly solved. Information privacy of local IBR information may be an important factor however, and we therefore consider a distributed method solution in which more information is kept local to each LCA. Define the closed convex constraint sets

$$\mathcal{C}_{\text{bal}} := \{(a_1, \dots, a_N) \mid (12b) \text{ holds}\}$$

$$\mathcal{C}_i := \{a_i \mid (12c) \text{ and } (12d) \text{ hold}\},$$

and let $\mathbb{I}_{\mathcal{C}}(x)$ denote the *indicator function* of a closed convex set \mathcal{C} , which is $+\infty$ if $x \in \mathcal{C}$ and zero otherwise. The problem (12) can be equivalently written as

$$\begin{aligned} & \min_{\{a_i\}_{i \in \mathcal{A}}} \sum_{i \in \mathcal{A}} [q_i a_i^2 + \mathbb{I}_{\mathcal{C}_i}(a_i)] + \mathbb{I}_{\mathcal{C}_{\text{bal}}}(z_1, \dots, z_N) \\ & \text{subject to } z_i = a_i, \quad i \in \mathcal{A}, \end{aligned}$$

where dummy variables z_i have been introduced. When written in this form, the problem now admits an iterative distributed solution via the *alternating direction method of multipliers* (ADMM) [42]. Each LCA receives the scalar computation variables (z_i^k, u_i^k) from the central controller, and locally computes a scalar update via the local optimization

$$a_i^{k+1} = \underset{a_i \in \mathbb{R}}{\operatorname{argmin}} \quad q_i a_i^2 + \mathbb{I}_{C_i}(a_i) + \frac{\rho}{2} |a_i - z_i^k + u_i^k|^2, \quad (14)$$

where $\rho > 0$ is a penalty parameter. The value a_i^{k+1} is returned to the central controller, which performs the vectorized coordination update

$$\begin{aligned} z^{k+1} &= \operatorname{Proj}_{C_{\text{bal}}}(\hat{a}^{k+1} + u^k) \\ u^{k+1} &= u^k + \hat{a}^{k+1} - z^{k+1}, \end{aligned} \quad (15)$$

where Proj denotes the Euclidean projection onto the constraint set. The update (14) is a small convex quadratic program, while (15) is just a linear update; both can be solved quickly and reliably, and the iterates a_i^k will converge to the optimizer of (12). The following parameters are communicated from the LCAs to the central controller: (i) the power mismatch φ_i in the LCA, (ii) the estimate $\Delta \hat{P}_{u,i}^k$ of the net power imbalance in the LCA, and (iii) the current power adjustment from the LCA a_i^{k+1} during the ADMM loop iteration process. The central controller in turn sends a weight vector $([w_j])$, which is computed from the estimated load imbalances, a control flag indicating convergence, and the iteration variables (z_i^{k+1}, u_i^{k+1}) . Communication occurs only between each LCA and the central coordinating control; LCAs do not communicate directly with one another. Hence, potentially sensitive information such as unit operating status, device limits, set-points, and available spare capacity of resources in an LCA are not shared with either the central controller or the LCA neighbors.

Remark III.1 (IBR Energy Sources and Markets). *In this work we have not focused on the specific energy sources behind the dc links of the IBRs, but have considered a generic source, which could be dispatchable integrated battery + inverter-based resource solutions [43], or dispatchable active power controlled wind farms [44], [45], [46], photovoltaic (PV) systems [16], [17], or a combination. For our purposes, the key feature is that the source is dispatchable within specified limits, which may themselves change over time. It is pertinent to note that the technology already exists for these IBRs to be dispatchable [10], [45].*

The controllers we design for each LCA require the IBRs to follow power set-point commands with limits. In the language of the current system, this is most similar to the concept of secondary frequency response reserves. We have assumed that these reserves can be quickly deployed, and have modelled a ramp time constant of 0.3 seconds for the IBRs used in our case studies. Determining the specific regulatory or market mechanism for providing such an ancillary service is outside the scope of this work, but is a topic of current consideration in the literature [45], [11], [47], [44], [48], [10]. Instead, we have assumed that dedicated IBRs with secondary frequency reserves are available in each LCA, and that these IBRs

send their current set-points and device information, including limits, to the LCA controller. The capacity and performance-based compensation to the IBRs for providing these reserves could be procured through long term agreements similar to those for voltage support ancillary service [49]. Finally, we remark that we do not envisage that these dedicated IBRs will be providing power indefinitely after a frequency event. On a longer time-scale, generators can be ramped up through the usual AGC system and IBR injections can be correspondingly ramped down to pre-event values, freeing up fast resources for future frequency events. \square

IV. SIMULATION STUDIES

We illustrate our designs by applying them to the 3-LCA 9-machine power system shown in Figure 1 and the 5-LCA 68-bus system shown in Figure 13, both implemented in Simscape Electrical. Each LCA of the interconnected system in Figure 1 is based on the IEEE 3-machine 9-bus system [50], with the areas interconnected through identical tie-lines, whose parameters are given in Table I.

TABLE I: Tie-line parameters for 3-area system; 100 megavolts ampere (MVA) base.

Node 1	Node 2	R (p.u.)	X (p.u.)	B (p.u.)
1	15	0.05	0.20	0.15
5	9	0.05	0.20	0.15
7	17	0.05	0.20	0.15

In total, four out of the initial nine synchronous generators in the 3-LCA system have been replaced with an equal number of lower-inertia wind power farms, with the majority of the active power in the modified system now being supplied by renewable power generation. The larger power system in Figure 13 is the 5-area 68-bus IEEE benchmark model, with 16 synchronous generators and 86 transmission lines from [51]. All of the conventional power plants were modelled with sixth-order synchronous generators and includes detailed turbine-governor, excitation, and power system stabilizer (PSS) models, while the wind power was modelled using Type 3, doubly-fed induction generator (DFIG) wind turbine systems. Two converter-based units, with droop control schemes, are present in each LCA for fast control, and include current limiters; system data is shown in Table II. In selecting suitable test systems for this work, we have modified the 3-LCA 9-machine system to better represent the low-inertia, green next-generation power grid, while the larger 5-LCA system represents a more conventional grid with slower frequency dynamics owing to the predominance of SGs over inverter-based power resources.

Each LCA disturbance estimator was designed based on the SFR model (10), with raw parameters taken from [50] and SFR parameters set based on the method in [37]. For the estimator design itself, time delays for both measurement and control signals were fixed at 200ms, and the estimator gain \mathcal{L} was tuned using standard linear-quadratic methods. Simulation tests were performed with measurement and control signal delays of 300ms and 500ms. The selection of 300 to 500ms

TABLE II: Generator and IBR Data.

Node	Gen. ID (and type)	Rating (MVA)	Dispatch (MW)
1,13	G1, G7 (Hydro)	247.50	72.24
1	IBR2 (Inverter-based resource)	50	15
3	G2 (Fossil-based)	192	126
3	IBR1 (Inverter-based resource)	50	25
5, 11, 17	G3, G6, G9 (Fossil-based)	128	85
7	G4 (Hydro)	247.5	71.99
7	IBR4 (Inverter-based resource)	50	20
9	G5 (Fossil-based)	192	133
11	IBR3 (Inverter-based resource)	50	10
13	IBR6 (inverter-based resource)	50	5
15	G8 (Fossil-based)	192	128
17	IBR5 (Inverter-based resource)	50	30

delays is a somewhat pessimistic choice, based on worst-case delays for wide-area communication via high-speed Ethernet.

Both the LCA controllers in Section II and the central controller in Section III operate continuously with a fixed sampling period $T_s = 25\text{ms}$, which was selected based on what can be expected based on continued deployment of PMUs. At each sampling period the LCA controllers send the power mismatch φ_i^* to the central controller, which computes the total power mismatch $\sum_{i \in \mathcal{A}} \varphi_i^*$. If this is within a pre-defined tolerance ($\approx 5\%$ of the spare capacity available in each area), then no further action is taken. When $\sum_{i \in \mathcal{A}} \varphi_i^*$ exceeds the set tolerance, a flag is triggered and the centralized optimization in Section III is executed, either by directly solving (12) when information is centralized, or by beginning the iterations (14)–(15) when information privacy must be preserved.

TABLE III: SFR model parameters for LCA estimator design.

Quantity	Value	Comment
H	Varies	Normalized area inertia constant
T_R	10 s	Reheat time constant
R_g, R_l	5%	Speed regulation
F_H	0.64	Frac. of power generated by high pressure turb.
D	0	Load damping coefficient
T_s	25 ms	Estimator sampling period
ϵ	10^{-9}	Avoids division by zero in (13)
λ	100	Penalty coefficient in (11)
ρ	1	Penalty coefficient in (14)

In total we consider seven scenarios, where the first six scenarios are simulated on the three-LCA power system shown in Figure 1 and the last scenario involving two cases is validated on a larger five-LCA power system shown in Figure 13. The scenarios considered include: (i) a step load change in one LCA of the three-LCA system that can be fully compensated with only local resources, (ii) a larger step load change in the same LCA, where support from the other areas will be required, (iii) a symmetric three phase-to-ground fault, (iv) the loss of a generator, (v) the intentional introduction of extreme variations in the parameters used in the LCA estimator designs for all three LCAs, (vi) the redispatching of both synchronous generators and IBRs in response to a load change, and (vii) the re-simulation of scenarios I and II on the larger five-LCA power system.

All scenarios are compared against a baseline case without our supplementary control scheme, wherein frequency support is provided only by conventional generators' inertia and by primary droop control action of both generators and IBRs. We

emphasize that our scheme does not aim to supplant the primary control actions of the active power generating resources (which are mandated by regulations from system operators), nor does our scheme attempt to emulate conventional generator inertia. Instead, our scheme is an alternative proposal for how IBRs can enable fast frequency control.

A. Scenario #1: Disturbance with Sufficient Local Resources

In this scenario, a 63 megawatts (MW) load change is applied at bus 8 in area two at $t = 2\text{s}$. The disturbance is sufficiently small such that it can be compensated locally without coordination with other areas. The frequency response and IBR power setpoints are plotted in Figure 3, where we additionally compare the response to that obtained by augmenting the conventional droop-only with an aggressively-tuned AGC-type control which redistributes the IBRs.

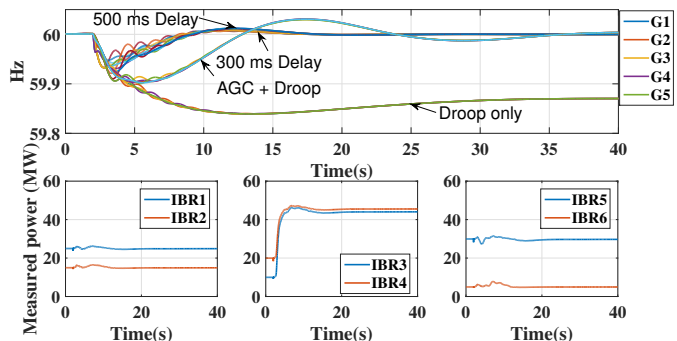


Fig. 3: Response to 63 MW load change at bus 8; the IBR power plots correspond to the case of 300ms delay.

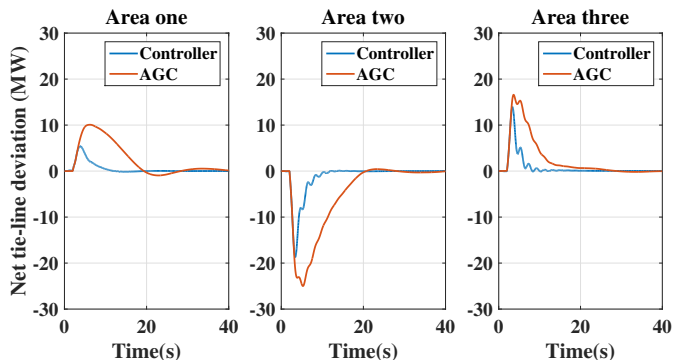


Fig. 4: Tie-line power flow deviations following a 63 MW load change at bus 8 in area two.

The frequency nadir and settling time with our controller is significantly improved compared to a conventional AGC + droop strategy, with similar performance observed up to 600ms of delay. The IBRs in area 2 quickly ramp up to compensate the disturbance, while the IBRs in areas 1 and 3 do not significantly respond; the control action is fast and localized. As one would expect, the closed-loop performance of the scheme degrades slightly with increasing delay; since however we have explicitly included an expectation of 200ms of delay in the design phase (Section II-A), the typical destabilizing effect of delays is largely mitigated.

Recall from Section II-A that each LCA controller is designed and implemented in an area-by-area decentralized fashion. In Figure 3, one can observe a slight increase in *inter-area* oscillations in the presence of our controller. A small-signal stability analysis was performed on the interconnected system, and we have observed a trade-off between the speed of the controller response and a degradation of the damping ration of this particular inter-area mode. This is perhaps not surprising, as the generator PSS units were tuned in the absence of our retrofit control scheme. If desired, this mode can be further damped by (i) re-tuning the PSS loops, or (ii) lowering the bandwidth of our control scheme, as described in Remark II.2.

In Figure 4, we observe that the proposed scheme reduces the inadvertent power exchange from adjacent areas following the disturbance compared to the classical AGC-balancing mechanism. In this scenario where the contingent area has sufficient resources to correct the local imbalance, the proposed scheme results in significantly less energy borrowed from adjacent areas, thereby minimizing any incurred penalty and providing additional value to the operator.

B. Scenario #2: Disturbance with Insufficient Local Resources

This scenario is identical to the self-sufficient case, but a 130 MW load change is applied instead, which is sufficiently large to activate both stage one and stage two of our redispatch scheme. The dynamic responses for this case are shown in Figure 5.

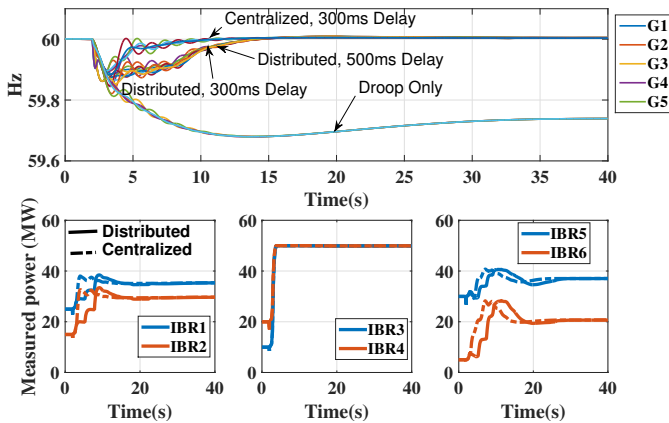


Fig. 5: Response to 130 MW load change at bus 8.

Following the disturbance, the controller in the contingent area reacts and maxes out its IBR resources, which both have limits of 50 MW; as expected, the controllers in other areas do not initially respond. Stage two activates after the total mismatch exceeds the specified tolerance of 20 MW; we plot the responses for both the centralized and distributed implementations of stage two (Section III-C). As can be seen in Figure 5, the non-contingent areas supply additional active power to compensate for the disturbance, and the system frequency is eventually brought back to nominal value. We have considered a communication delay of 300 ms for the centralized implementation and both 300 ms and 500 ms delays for the distributed implementation. As the distributed

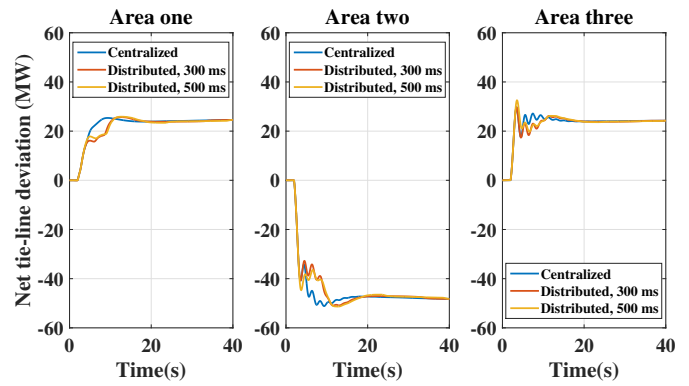


Fig. 6: Plot of net tie-line flows following a 130 MW load change at bus 8.

implementation requires many iterations, each of which is subject to communication delays, it is noticeably slower than the centralized implementation. The responses therefore illustrate the speed-privacy trade-off between the centralized and distributed implementations. The net tie-line deviations from pre-disturbance values are plotted in Figure 6; a comparison with an AGC-type control has not been included in this case since, due to the insufficient IBRs’ capacity in the contingent area, it will be impossible for the integral control of the AGC to restore the tie-line flows to their scheduled values.

C. Scenario #3: Symmetric Three-Phase Fault

For this scenario, a three-phase line-to-ground fault was introduced at bus 10 in area 2 at $t = 2$ s; the fault was cleared after 0.1 secs. Figures 7 and 8 show the dynamic response of the system following the introduction of the fault.

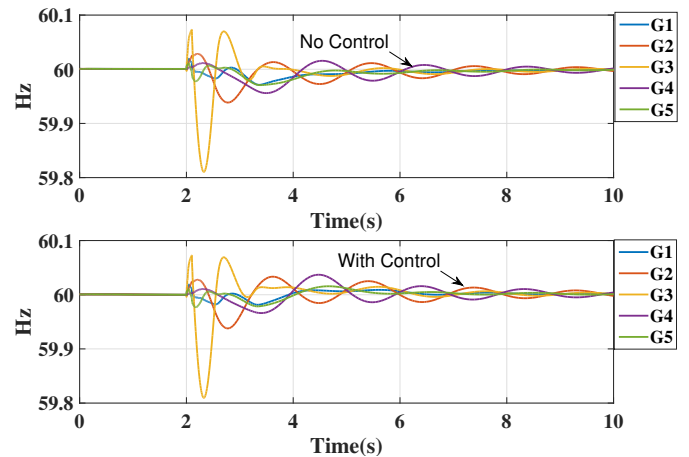


Fig. 7: Frequency response to three-phase fault.

From Figure 7, we see that our design does not alter the transient frequency behaviour of the system following the fault compared to the base case. As can be seen from Figure 8, the load estimates in the non-contingent areas are negligible, and the IBRs do not significantly respond. In the contingent area there is a small transient disturbance estimate, which smoothly returns to zero with minimal IBR response. We conclude that

the control strategy is able to detect ‘frequency events’ and ignore ‘non-frequency events’, which are desirable properties of fast frequency response schemes [5].

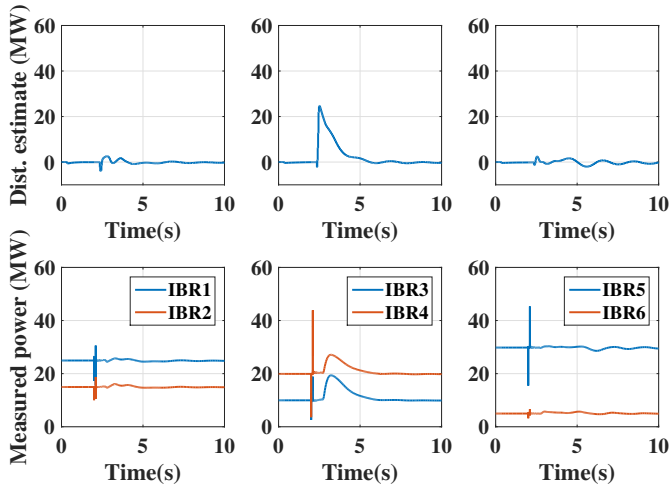


Fig. 8: Plots of load estimate and IBR outputs following a three-phase line-to-ground fault at bus 8 in area 2.

D. Scenario #4: Loss of Generator

In this scenario, we have simulated a loss of generator G2 in area 2 at $t = 2$ s. The lost generator had a pre-fault dispatch of ≈ 72 MW. The response is plotted in Figure 9. Similar to

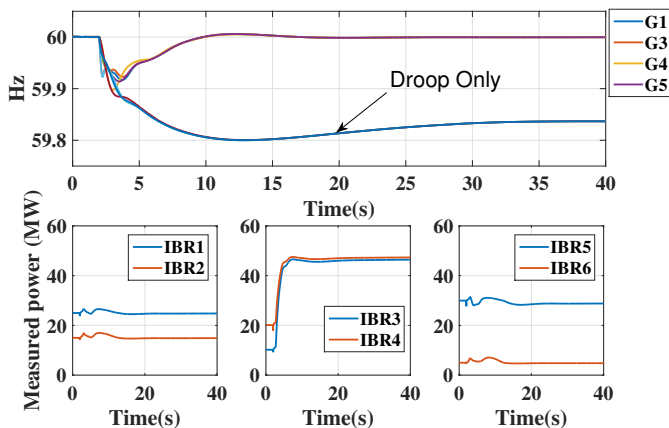


Fig. 9: Response to loss of generator G2.

Scenario #2, the controller in the contingent area maxes out its IBR resources following the generator loss, which resulted in a load imbalance of ~ 72 MW. Controllers in other areas however do not provide additional support via stage two, as the remaining power mismatch does not exceed the specified tolerance of 20 MW. This scenario additionally illustrates the robustness of the method, as the LCA controller for area 2 is designed assuming that the inertia and primary response of generator G2 are present. Despite this significant parameter variation, the control action is similar to that in Scenario #1.

E. Scenario #5: Parameter Variation

In this scenario we assess the controller’s performance in the presence of extreme variations in the parameters used in the LCA estimator designs for all three areas; see Table IV. The disturbance is as in Scenario #1, with a communication delay of 300ms. The response is shown in Figure 10.

TABLE IV: SFR model parameters for Scenario #5.

Case	Quantity	Value
Base Case	H	nominal
	T_R	nominal
	R_g	nominal
	R_l	nominal
	F_H	nominal
Case 1	H	50% decrease from nominal
	T_R	80% decrease from nominal
	R_g	50% decrease from nominal
	R_l	50% decrease from nominal
	F_H	Same as nominal
Case 2	H	50% decrease from nominal
	T_R	60% increase over nominal
	R_g	10% increase over nominal
	R_l	10% increase over nominal
	F_H	65% decrease from nominal

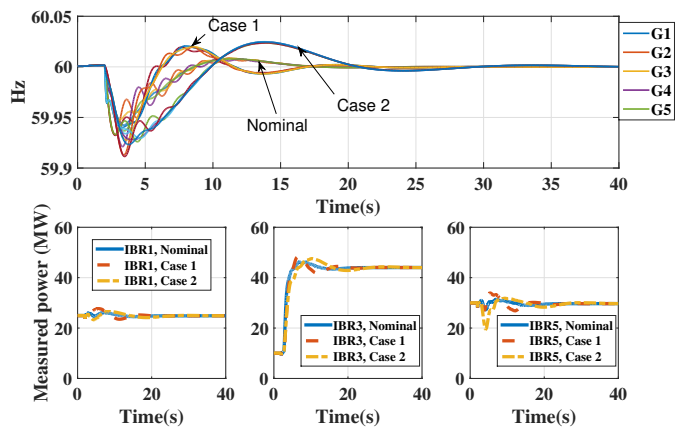


Fig. 10: Response with variations in model parameters.

It can be seen from Figure 10 that the system remains stable despite these significant parameter variations, although the frequency response is degraded. Case 1 produces a more oscillatory response due to the underestimated turbine time constant, while Case 2 produces a larger overshoot due to the overestimated turbine constant. Consequently, this scenario illustrates the margin of error we are afforded in the model used for the LCA estimator design.

F. Scenario #6: Coordination of IBRs and Conventional Generators

While our control scheme is primarily intended for coordination and dispatch of fast IBRs, the optimal redispatch in Section III-A is in fact agnostic to the underlying source of power used to correct the imbalance. To illustrate the modularity and flexibility of our approach, in this scenario we consider both the conventional synchronous generators (SGs) and the IBRs in the optimal active power allocation of Section III-A. The ratings of the SGs are as shown in Table II, while the capacities of the IBRs were increased to 100 MVA to

encourage more IBR participation for this particular test. A 63MW load change is applied at bus 8 in area two at $t = 2s$, and the system responses are shown in Figures 11, 12. Both IBRs and SGs are jointly redispatched according to Section III-A; due to the slower response speed of SGs, the overall speed of the scheme is reduced compared to compensation using only IBRs. In summary, while SGs can be directly integrated into the proposed scheme, this will not necessarily lead to improved performance.

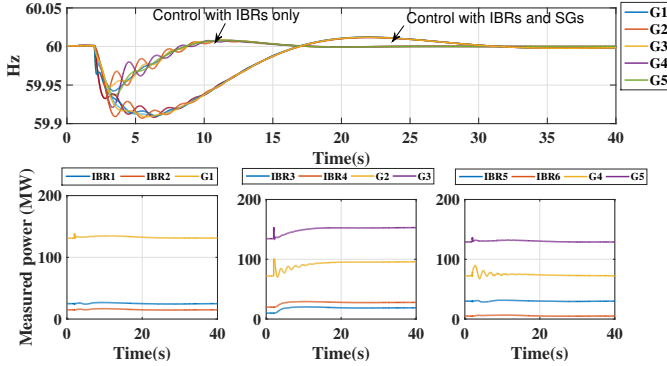


Fig. 11: Response to 63MW load change at bus 8 with redispatch of both SGs and IBRs.

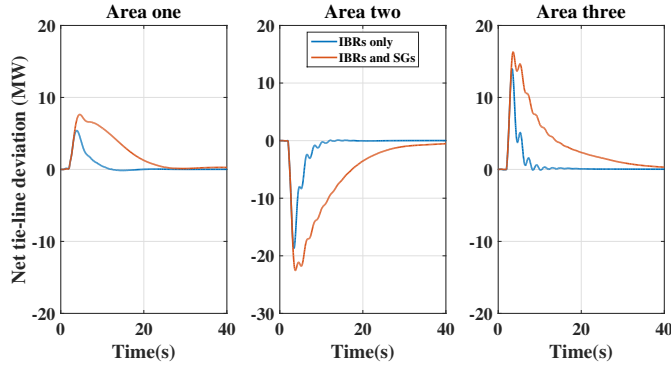


Fig. 12: Plot of net tie-line flows following a 63 MW load change at bus 8 with redispatch of both SGs and IBRs.

G. Scenario #7: Test on Larger Power System

To test the performance of the proposed scheme on a large power system, we repeat self sufficient and deficient scenarios (Scenarios #1 and #2) on the 5-LCA test system shown in Figure 13.

For the self sufficient case, we introduce a 300 MW load change at bus 33 in the NYPS area at $t = 2s$. The frequency response, IBR power setpoints and net tie-line deviations are plotted in Figures 14, 15. It can be seen that the performance is similar to that obtained in the smaller 3-area system (Section IV-A), with the IBRs in the contingent area acting quickly to inject active power while those in the non-contingent areas remain close to their dispatch values, resulting in the restoration of the frequency and net tie-line deviations to their pre-disturbance values significantly faster than an aggressively tuned traditional AGC. The controller

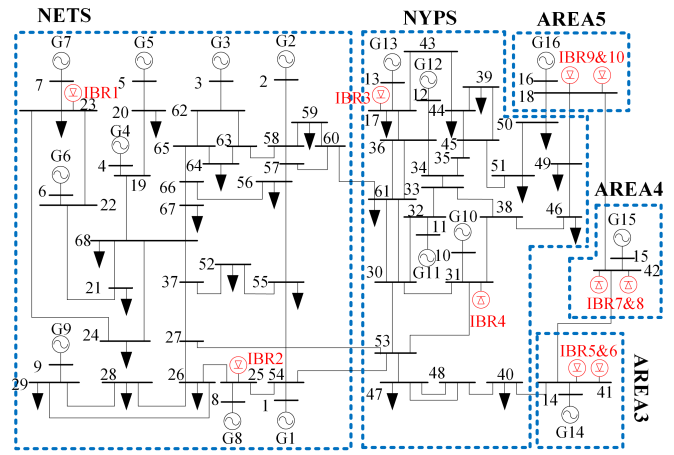


Fig. 13: 5-area 68-bus test system.

shows good performance for both the 300 ms and 500 ms communication delays simulated. From Figure 15, we see that the scheme quickly restores the tie line power flows to their pre-disturbance values compared to the AGC-type scheme, minimizing inadvertent exchange between LCAs.

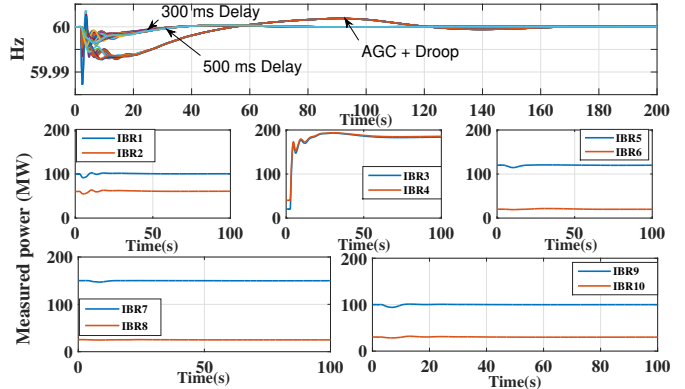


Fig. 14: Response to 300 MW load change at bus 33.

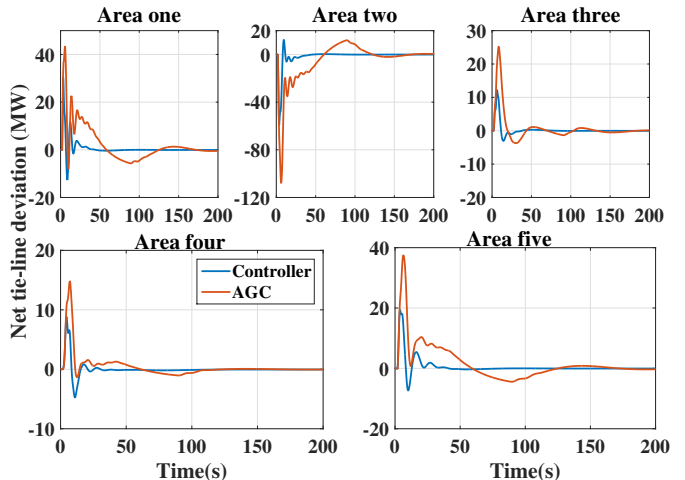


Fig. 15: Plot of net tie-line flows following a 300 MW load change at bus 33.

We next consider the case where the resources in the contingent area are insufficient to correct a local load imbalance. Here, we introduce a 450 MW load change at bus 33 in the NYPS area at $t = 2$ s. As can be seen in Figures 16, 17, the non-contingent areas supply additional active power to compensate for the disturbance after the IBRs in the contingent areas reach their limit and stage two is activated. Since the NETS area and area 5 are electrically closest to NYPS, more active power is sourced from them. The conclusions drawn in Section IV-B still hold on the larger 68-bus system, with the centralized implementation being slightly faster and the controller showing robust performance under the simulated 300 ms and 500 ms communication delays scenarios.

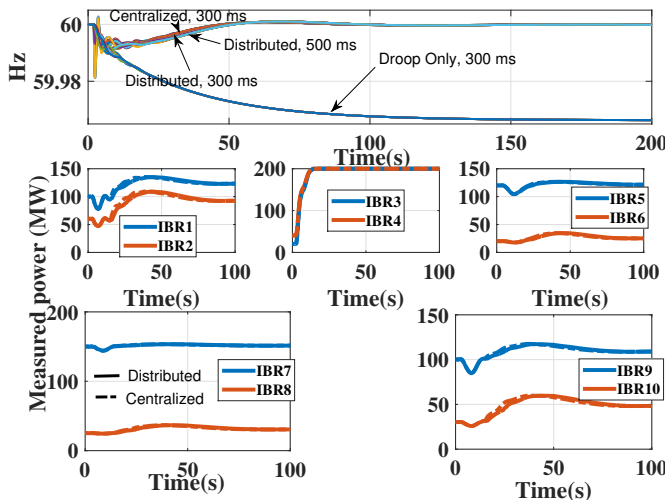


Fig. 16: Response to 450 MW load change at bus 33.

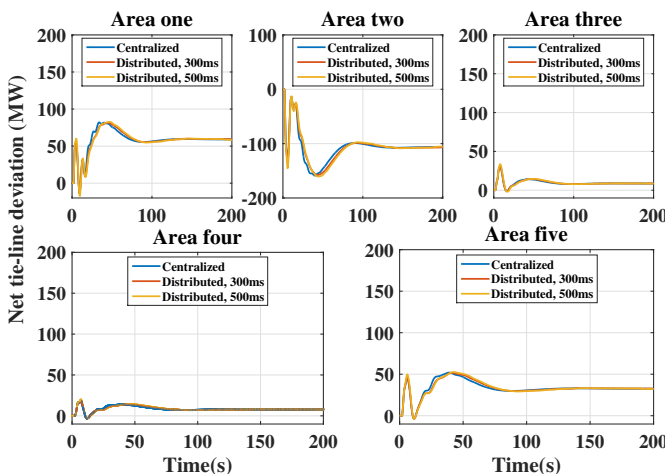


Fig. 17: Plot of net tie-line flows following a 450 MW load change at bus 33.

V. CONCLUSIONS

We have proposed and validated through detailed simulations a control strategy that provides fast, localized frequency control by partitioning the power system into small areas, and utilizing the fast, inverter-based resources in each area to correct load imbalances originating locally. The local control loop

for each LCA quickly estimates the local disturbance and compensates by re-dispatching IBRs. When required, additional power support from neighboring areas is provided from electrically close areas using a higher-level coordinated dispatch scheme, and we propose a privacy-preserving implementation for this layer. The approach provides fast control action and can be retrofit onto existing systems without compromising stability. Through the LCA controllers, the scheme explicitly accounts for heterogeneity of inertial response throughout the power system.

Directions for future research include adaptive and data-driven extensions of this framework for improved disturbance estimation in practice. Furthermore, we would also seek to improve the implementation of stage two by investigating the viability, quantifying performance limits, and assessing communication and measurement requirements of using a peer-to-peer based strategy for additional power support. Finally, for the purposes of this work, we have assumed that the area partitions are already given. However, an additional open question is how to optimally partition the system into areas which are appropriate for this decentralized control architecture.

REFERENCES

- [1] IRENA, “Global energy transformation: A roadmap to 2050,” 2018.
- [2] A. Ulbig, T. S. Borsche, and G. Andersson, “Impact of Low Rotational Inertia on Power System Stability and Operation,” in *IFAC World Congress*, vol. 47, (Cape Town, South Africa), pp. 7290–7297, Aug. 2014.
- [3] F. Milano, F. Dörfler, G. Hug, D. J. Hill, and G. Verbič, “Foundations and challenges of low-inertia systems,” in *Power Systems Computation Conference*, pp. 1–25, 2018.
- [4] B. K. Poolla, S. Bolognani, and F. Dörfler, “Optimal placement of virtual inertia in power grids,” *IEEE Transactions on Automatic Control*, vol. 62, no. 12, pp. 6209–6220, 2017.
- [5] Q. Hong, M. Nedd, S. Norris, I. Abdulhadi, M. Karimi, V. Terzija, B. Marshall, K. Bell, and C. Booth, “Fast frequency response for effective frequency control in power systems with low inertia,” *The Journal of Engineering*, vol. 2019, no. 16, pp. 1696–1702, 2019.
- [6] R. Yan, T. K. Saha, F. Bai, H. Gu, *et al.*, “The anatomy of the 2016 south australia blackout: A catastrophic event in a high renewable network,” *IEEE Transactions on Power Systems*, vol. 33, no. 5, pp. 5374–5388, 2018.
- [7] E. Ekomwenrenren, H. Alharbi, T. Elgorashi, J. Elmighani, and P. Aristidou, “Stabilising control strategy for cyber-physical power systems,” *IET Cyber-Physical Systems: Theory & Applications*, vol. 4, no. 3, pp. 265–275, 2019.
- [8] A. Chakraborty, “Wide-area communication and control: A cyber-physical perspective,” in *Smart Grid Control*, pp. 139–164, Springer, 2019.
- [9] G. Papaefthymiou and K. Dragoon, “Towards 100% renewable energy systems: Uncapping power system flexibility,” *Energy Policy*, vol. 92, pp. 69–82, 2016.
- [10] F. Van Hulle, H. Holttinen, J. Kiviluoma, M. Faiella, P. Kreutzkamp, N. Cutululis, M. Reisinger, A. Gubina, F. Chapalain, B. Ernst, S. Wachtel, G. Quinonez Varela, D. Craciun, I. Pineda, B. Stoffer, J. Corbett, and A. Flament, *Grid support services by wind and solar PV: a review of system needs, technology options, economic benefits and suitable market mechanisms: Synthesis report of the REServiceS project*. 2014.
- [11] A. Banswar, N. K. Sharma, Y. R. Sood, and R. Shrivastava, “Renewable energy sources as a new participant in ancillary service markets,” *Energy strategy reviews*, vol. 18, pp. 106–120, 2017.
- [12] A. Pappachen and A. P. Fathima, “Critical research areas on load frequency control issues in a deregulated power system: A state-of-the-art-of-review,” *Renewable and Sustainable Energy Reviews*, vol. 72, pp. 163–177, 2017.

- [13] A. Adrees, J. Milanović, and P. Mancarella, “Effect of inertia heterogeneity on frequency dynamics of low-inertia power systems,” *IET Generation, Transmission & Distribution*, vol. 13, no. 14, pp. 2951–2958, 2019.
- [14] A. E. Leon, “Short-term frequency regulation and inertia emulation using an mmc-based mtdc system,” *IEEE Transactions on Power Systems*, vol. 33, no. 3, pp. 2854–2863, 2017.
- [15] O. D. Adeuyi, M. Cheah-Mane, J. Liang, and N. Jenkins, “Fast frequency response from offshore multiterminal vsc-hvdc schemes,” *IEEE Transactions on Power Delivery*, vol. 32, no. 6, pp. 2442–2452, 2016.
- [16] H. Xin, Y. Liu, Z. Wang, D. Gan, and T. Yang, “A new frequency regulation strategy for photovoltaic systems without energy storage,” *IEEE Transactions on Sustainable Energy*, vol. 4, no. 4, pp. 985–993, 2013.
- [17] A. F. Hoke, M. Shirazi, S. Chakraborty, E. Muljadi, and D. Maksimovic, “Rapid active power control of photovoltaic systems for grid frequency support,” *IEEE Journal of Emerging and Selected Topics in Power Electronics*, vol. 5, no. 3, pp. 1154–1163, 2017.
- [18] D. Yang, J. Kim, Y. C. Kang, E. Muljadi, N. Zhang, J. Hong, S.-H. Song, and T. Zheng, “Temporary frequency support of a dfig for high wind power penetration,” *IEEE Transactions on Power Systems*, vol. 33, no. 3, pp. 3428–3437, 2018.
- [19] D. Ochoa and S. Martinez, “Fast-frequency response provided by dfig-wind turbines and its impact on the grid,” *IEEE Transactions on Power Systems*, vol. 32, no. 5, pp. 4002–4011, 2016.
- [20] T. Xu, W. Jang, and T. Overbye, “Commitment of fast-responding storage devices to mimic inertia for the enhancement of primary frequency response,” *IEEE Transactions on Power Systems*, vol. 33, no. 2, pp. 1219–1230, 2017.
- [21] Y. Tan, K. M. Muttaqi, P. Ciufu, L. Meegahapola, X. Guo, B. Chen, and H. Chen, “Enhanced frequency regulation using multilevel energy storage in remote area power supply systems,” *IEEE Transactions on Power Systems*, vol. 34, no. 1, pp. 163–170, 2018.
- [22] A. N. Venkat, I. A. Hiskens, J. B. Rawlings, and S. J. Wright, “Distributed mpc strategies with application to power system automatic generation control,” *IEEE Transactions on Control Systems Technology*, vol. 16, no. 6, pp. 1192–1206, 2008.
- [23] A. M. Ersdal, L. Inslund, and K. Uhlen, “Model predictive load-frequency control,” *IEEE Transactions on Power Systems*, vol. 31, no. 1, pp. 777–785, 2015.
- [24] J. Köhler, M. A. Müller, N. Li, and F. Allgöwer, “Real time economic dispatch for power networks: A distributed economic model predictive control approach,” in *IEEE Conf. on Decision and Control*, (Melbourne, Australia), pp. 6340–6345, 2017.
- [25] P. R. B. Monasterios and P. Trodden, “Low-complexity distributed predictive automatic generation control with guaranteed properties,” *IEEE Transactions on Smart Grid*, vol. 8, no. 6, pp. 3045–3054, 2017.
- [26] N. Li, C. Zhao, and L. Chen, “Connecting automatic generation control and economic dispatch from an optimization view,” *IEEE Transactions on Control of Network Systems*, vol. 3, pp. 254–264, Sept. 2016.
- [27] D. Apostolopoulou, P. W. Sauer, and A. D. Domuez-García, “Balancing authority area model and its application to the design of adaptive AGC systems,” *IEEE Transactions on Power Systems*, vol. 31, no. 5, pp. 3756–3764, 2016.
- [28] L. Olmos, J. I. de la Fuente, J. Z. Macho, R. R. Pecharromán, A. M. Calmarza, and J. Moreno, “New design for the spanish agc scheme using an adaptive gain controller,” *IEEE Transactions on Power Systems*, vol. 19, no. 3, pp. 1528–1537, 2004.
- [29] L. Dong, Y. Tang, H. He, and C. Sun, “An event-triggered approach for load frequency control with supplementary adp,” *IEEE Transactions on Power Systems*, vol. 32, no. 1, pp. 581–589, 2016.
- [30] B. D. Anderson *et al.*, “Failures of adaptive control theory and their resolution,” *Communications in Information & Systems*, vol. 5, no. 1, pp. 1–20, 2005.
- [31] A. M. Prostejovsky, M. Marinelli, M. Rezkalla, M. H. Syed, and E. Guillo-Sansano, “Tuningless load frequency control through active engagement of distributed resources,” *IEEE Transactions on Power Systems*, vol. 33, no. 3, pp. 2929–2939, 2017.
- [32] P. Wall, N. Shams, V. Terzija, V. Hamidi, C. Grant, D. Wilson, S. Norris, K. Maleka, C. Booth, Q. Hong, *et al.*, “Smart frequency control for the future gb power system,” in *IEEE PES Innovative Smart Grid Technologies Conference Europe*, pp. 1–6, 2016.
- [33] M. Morari and E. Zafiriou, *Robust process control*. Chemical Engineering Research and Design. Prentice Hall, 1987.
- [34] E. Davison, “The robust control of a servomechanism problem for linear time-invariant multivariable systems,” *IEEE Transactions on Automatic Control*, vol. 21, no. 1, pp. 25–34, 1976.
- [35] A. Isidori, *Lectures in feedback design for multivariable systems*, vol. 3. Springer, 2017.
- [36] W. S. Levine, *The Control Systems Handbook: Control System Advanced Methods*. CRC press, 2018.
- [37] P. M. Anderson and M. Mirheydar, “A low-order system frequency response model,” *IEEE Transactions on Power Systems*, vol. 5, no. 3, pp. 720–729, 1990.
- [38] H. Min, F. Paganini, and E. Mallada, “Accurate reduced order models for coherent synchronous generators,” in *2019 57th Annual Allerton Conference on Communication, Control, and Computing (Allerton)*, pp. 316–317, IEEE, 2019.
- [39] U. Markovic, Z. Chu, P. Aristidou, and G. Hug, “Lqr-based adaptive virtual synchronous machine for power systems with high inverter penetration,” *IEEE Transactions on Sustainable Energy*, vol. 10, no. 3, pp. 1501–1512, 2018.
- [40] J. Veenman, C. W. Scherer, and H. Köroğlu, “Robust stability and performance analysis based on integral quadratic constraints,” *European Journal of Control*, vol. 31, pp. 1–32, 2016.
- [41] F. Dörfler and F. Bullo, “Kron reduction of graphs with applications to electrical networks,” *IEEE Transactions on Circuits and Systems I: Fundamental Theory and Applications*, vol. 60, no. 1, pp. 150–163, 2012.
- [42] D. K. Molzahn, F. Dörfler, H. Sandberg, S. H. Low, S. Chakrabarti, R. Baldick, and J. Lavaei, “A survey of distributed optimization and control algorithms for electric power systems,” *IEEE Transactions on Smart Grid*, vol. 8, no. 6, pp. 2941–2962, 2017.
- [43] S. Teleke, M. E. Baran, S. Bhattacharya, and A. Q. Huang, “Rule-based control of battery energy storage for dispatching intermittent renewable sources,” *IEEE Transactions on Sustainable Energy*, vol. 1, no. 3, pp. 117–124, 2010.
- [44] M. Braun, *Provision of Ancillary Services by Distributed Generators: Technological and Economic Perspective*. Erneuerbare Energien und Energieeffizienz, Kassel University Press, 2009.
- [45] J. Aho, A. Buckspan, J. Laks, P. Fleming, Y. Jeong, F. Dunne, M. Churchfield, L. Pao, and K. Johnson, “A tutorial of wind turbine control for supporting grid frequency through active power control,” in *2012 American Control Conference (ACC)*, pp. 3120–3131, IEEE, 2012.
- [46] R. E. de España *et al.*, “Transmission system operation with a large penetration of wind and other renewable electricity sources in electricity networks using innovative tools and integrated energy solutions (twenties),” tech. rep., Madrid, Spain, Final Rep., Oct, 2013.
- [47] A. D. Papalexopoulos and P. E. Andrianesis, “Performance-based pricing of frequency regulation in electricity markets,” *IEEE Transactions on Power systems*, vol. 29, no. 1, pp. 441–449, 2012.
- [48] E. Ela, V. Gevorgian, A. Tuohy, B. Kirby, M. Milligan, and M. O’Malley, “Market designs for the primary frequency response ancillary service—part i: Motivation and design,” *IEEE Transactions on Power Systems*, vol. 29, no. 1, pp. 421–431, 2013.
- [49] Y. G. Rebours, D. S. Kirschen, M. Trotignon, and S. Rossignol, “A survey of frequency and voltage control ancillary services—part ii: Economic features,” *IEEE Transactions on power systems*, vol. 22, no. 1, pp. 358–366, 2007.
- [50] P. M. Anderson and A. A. Fouad, *Power system control and stability*. John Wiley & Sons, 2008.
- [51] B. Pal and B. Chaudhuri, *Robust control in power systems*. Springer Science & Business Media, 2006.

APPENDIX A PROOFS

Proof of Proposition II.1: A minimal state-space realization of an n -step time delay has matrices of the general form

$$A_m = \begin{bmatrix} 0 & \cdots & \cdots & 0 \\ I & \ddots & & \vdots \\ & & \ddots & \vdots \\ & & & I \end{bmatrix}, \quad B_m = \begin{bmatrix} I \\ 0 \\ \vdots \\ 0 \end{bmatrix}, \quad C_m = \begin{bmatrix} 0 \\ \vdots \\ 0 \\ I \end{bmatrix}^T,$$

Note that all eigenvalues of A_m are zero. By the PBH test [35], detectability of (C, A) is equivalent to the matrix $M := \begin{bmatrix} A - \lambda I \\ C \end{bmatrix}$ having full rank for all $\lambda \in \mathbb{C}$ with $|\lambda| \geq 1$. Direct substitution yields

$$M = \begin{bmatrix} A - \lambda I & B_2 & B_1 C_c & 0 \\ 0 & (1 - \lambda) & 0 & 0 \\ 0 & 0 & \mathcal{G}_1 & 0 \\ \begin{bmatrix} C \\ 0 \\ \vdots \\ 0 \\ 0 \end{bmatrix} & 0 & 0 & \mathcal{G}_2 \\ 0 & 0 & 0 & [0 \ 0 \ \dots \ 0 \ I] \end{bmatrix}$$

where

$$\mathcal{G}_1 = \mathcal{G}_2 := \begin{bmatrix} -\lambda I & 0 & \dots & 0 \\ I & -\lambda I & \ddots & \vdots \\ \vdots & \ddots & \ddots & 0 \\ 0 & \dots & I & -\lambda I \end{bmatrix}.$$

Using elementary row operations on the sub-matrices comprising of the 4th and 5th rows of M , we obtain

$$M \sim \begin{bmatrix} A - \lambda I & B_3 & B_1 C_c & 0 \\ 0 & (1 - \lambda) & 0 & 0 \\ 0 & 0 & \mathcal{G}_1 & 0 \\ C & 0 & 0 & 0 \\ 0 & 0 & 0 & I \end{bmatrix}.$$

Similarly, $[0 \ 0 \ \mathcal{G}_1 \ 0]$ can be row reduced to $[0 \ 0 \ I \ 0]$. By further interchanging the rows of the matrix, we obtain

$$M \sim \begin{bmatrix} A - \lambda I & B_2 & B_1 C_c & 0 \\ C & 0 & 0 & 0 \\ 0 & (1 - \lambda)I & 0 & 0 \\ 0 & 0 & I & 0 \\ 0 & 0 & 0 & I \end{bmatrix}$$

If $\lambda \neq 1$ but $|\lambda| > 1$, then the columns of the matrix are linearly independent if and only if $\begin{bmatrix} A - \lambda I \\ C \end{bmatrix}$ has full rank, which holds since A is Schur stable. If $\lambda = 1$, then M has full rank if and only if the submatrix $\begin{bmatrix} A - I & B_2 \\ C & 0 \end{bmatrix}$ has full rank, which holds by assumption. \square

Proof of Theorem II.3: Let $e_i = \widehat{\Delta P}_{u,i} - \Delta P_{u,i}$ denote the local estimation error with e and ΔP_u denoting the stacked vectors of errors and net-load disturbances. At the sampling instants, the closed-loop system with disturbance input ΔP_u and estimation error output e is described by a state-space model (A_F, B_F, C_F, D_F) where A_F is Schur stable, with associated $N \times N$ BIBO stable transfer matrix $H(z) = C_F(zI - A_F)^{-1}B_F + D_F$. It follows from the final value theorem that

$$\lim_{k \rightarrow \infty} e^k = \lim_{z \rightarrow 1} \frac{z-1}{z} H(z) \frac{z}{z-1} \Delta P_u = H(1) \Delta P_u.$$

We conclude that $\widehat{\Delta P}_{u,i}^k \rightarrow \Delta P_{u,i}$ as $k \rightarrow \infty$ for each $i \in \mathcal{A}$ and for any constant disturbances $\Delta P_{u,i}$ if and only if $H(1) = 0$. Define the Rosenbrock matrix $R(z) = \begin{bmatrix} zI - A_F & -B_F \\ C_F & D_F \end{bmatrix}$, and note the simple identity

$$\begin{bmatrix} I & 0 \\ -C_F(I - A_F)^{-1} & I \end{bmatrix} R(1) = \begin{bmatrix} I - A_F & -B_F \\ 0 & H(1) \end{bmatrix},$$

where the first matrix on the left is invertible (and well-defined since A_F is Schur stable). Since $I - A_F$ is invertible, it follows that $H(1) = 0$ if and only if $\text{rank}(R(1)) = \text{size}(A_F)$. Therefore, to establish our claim, we are going to show that $R(z)$ drops rank by N at $z = 1$.

Consider now the estimator (8) designed for the augmented dynamic LCA model (7). Without loss of generality, we neglect communication delays and remove the associated states. To further simplify the remainder of the proof, we neglect any IBR dynamics, which further implies that $B_i^1 = -B_i^2$. Under these assumptions, the estimator is written as

$$\begin{bmatrix} \Delta \hat{x}_i^{k+1} \\ \Delta \widehat{P}_{u,i}^{k+1} \end{bmatrix} = A_{o,i} \begin{bmatrix} \Delta \hat{x}_i^k \\ \Delta \widehat{P}_{u,i}^k \end{bmatrix} + B_{o,i} \begin{bmatrix} \Delta P_{\text{tie},i}^k \\ \Delta P_{\text{ibr,tot},i}^k \end{bmatrix} - \begin{bmatrix} L_i^1 \\ L_i^2 \end{bmatrix} \Delta y_i^k$$

where

$$A_{o,i} = \begin{bmatrix} A_i & B_i^2 \\ 0 & 1 \end{bmatrix} + \begin{bmatrix} L_i^1 \\ L_i^2 \end{bmatrix} \begin{bmatrix} C_i & 0 \end{bmatrix}, \quad B_{o,i} = \begin{bmatrix} B_i^2 & B_i^1 \\ 0 & 0 \end{bmatrix}$$

We let $C_{o,i} = [0 \ 1]$. The interconnected power system from the setup is represented as

$$\begin{aligned} \Delta x_p^{k+1} &= A_p \Delta x_p^k + \sum_{i \in \mathcal{A}} B_{p_i} (\Delta \widehat{P}_{u,i}^k - \Delta P_{u,i}) \\ \Delta y_{p,i}^k &= (\Delta P_{\text{tie},i}^k, \Delta y_i^k) = \begin{bmatrix} C_{p_i}^1 \\ C_{p_i}^2 \end{bmatrix} \Delta x_p^k, \end{aligned}$$

where we have made explicit the measurements used by the local estimators. Combining the equations, the closed-loop system matrices are given by

$$\begin{aligned} A_F &= \begin{bmatrix} A_p & [0 \ B_{p_1}] & \dots & [0 \ B_{p_N}] \\ B_{e_1} & A_{e_1} & \dots & \vdots \\ \vdots & \vdots & \ddots & 0 \\ B_{e_N} & 0 & 0 & A_{e_N} \end{bmatrix}, \quad D_F = -I_N \\ B_F &= \begin{bmatrix} -B_{p_1} & \dots & -B_{p_N} \\ 0 & 0 & 0 \\ \vdots & \vdots & \vdots \\ 0 & 0 & 0 \end{bmatrix}, \quad C_F = \begin{bmatrix} 0 & C_{o_1} & \dots & 0 \\ 0 & \vdots & \ddots & \vdots \\ 0 & 0 & \dots & C_{o_N} \end{bmatrix} \end{aligned}$$

where $B_{e_i} = \begin{bmatrix} B_i^2 \\ 0 \end{bmatrix} C_{p_i}^1 - \begin{bmatrix} L_i^1 \\ L_i^2 \end{bmatrix} C_{p_i}^2$ and

$$A_{e_i} = A_{o,i} + \begin{bmatrix} B_i^1 \\ 0 \end{bmatrix} C_{o_i} = \begin{bmatrix} A_i + L_i^1 C_i & 0 \\ L_i^2 C_i & 1 \end{bmatrix},$$

where we have used that $B_i^1 = -B_i^2$. Substitution now shows that $R(1)$ is given by

$$\left[\begin{array}{cccc|ccc} I - A_p & [0 \ -B_{p_1}] & \dots & [0 \ -B_{p_N}] & B_{p_1} & \dots & B_{p_N} \\ -B_{e_1} & J_1 & \dots & 0 & 0 & \dots & 0 \\ \vdots & \vdots & \ddots & 0 & \vdots & \vdots & \vdots \\ -B_{e_N} & 0 & 0 & J_N & 0 & 0 & 0 \\ \hline 0 & [0 \ 1] & \dots & 0 & -1 & \dots & 0 \\ 0 & \vdots & \ddots & \vdots & \dots & \ddots & \vdots \\ 0 & 0 & \dots & [0 \ -1] & 0 & \dots & -1 \end{array} \right]$$

where $J_i = I - A_{e_i} = \begin{bmatrix} I - (A_i + L_i^1 C_i) & 0 \\ L_i^2 C_i & 0 \end{bmatrix}$. By direct inspection, the third block column of the above is -1 times the $2N + 2$ nd block column, the fifth block column is -1 times $2N + 3$ rd block column, and so forth. It follows that the final N columns are redundant, which completes the proof. \square